This article has been accepted for publication in a future issue of this journal, but has not been fully edited. Content may change prior to final publication. Citation information: DOI 10.1109/TAP.2017.2677379, IEEE Transactions on Antennas and Propagation

5:1 Bandwidth Dielectric Rod Antenna using a Novel Feed Structure

Anas J. Abumunshar, *Student Member, IEEE,* and Kubilay Sertel, *Senior Member, IEEE*

***Abstract*— We present an ultra-wideband dielectric rod antenna using a novel V-shaped twin-wire tapered TEM waveguide as the feed structure. The new feed taper allows for much wider bandwidth and resolves the pattern-degradation in higher frequencies which is typically encountered in endfire mode dielectric rod antennas. The three sections of the antenna geometry, namely the feed taper, the rod body and the radiation taper are concurrently designed to achieve a 5:1 frequency bandwidth covering 6-30GHz, 17dB maximum gain and side lobe levels below -20dB over the entire band. The design is fabricated using Rexolit_1422 (epsilon_r=2.53) and measured performance is compared with simulation results, illustrating the effectiveness of the new feed structure in providing 5:1 bandwidth with stable radiation patterns within the entire band.**

***Index Terms*—Dielectric rod antenna, dual-polarization feed, ultra-wideband, ultra-wideband antenna.**

I. Introduction

The dielectric rod antenna, commonly known as "poly-rod", first appeared in 1939 [1] and is considered a special case of "surface wave" antennas, where the electromagnetic energy propagates on the inside, as well as the outside of the rod before it radiates at the terminal discontinuity of the rod surface. Due to their electrically long dimension, they are also considered as travelling-wave antennas. In general, such antennas achieve high gain over a broad bandwidth, making them attractive for ultra-wideband applications, such as ground penetrating radars. Moreover, dielectric rods are also popular due to their low side lobe levels, low radar-cross-section and high polarization purity. For instance, in near-field scanning probe applications, low radar cross section is critical in order to minimize the mutual coupling between the probe and the antenna under the test. In addition, a single broad beam is essential to minimize the effects of probe directivity and polarization purity for accurate near-to-far-field transformations [2] [3]. Furthermore, in other applications, such as reflector antennas, dielectric rods are used as the reflector feed as they enable reduced blockage and interference with the direct radiation from reflector. These unique features have led the dielectric rod antennas to be widely used in many applications and research continues to further improve performance, particularly for achieving wider bandwidth using a smaller footprint.

Circular cross sectional dielectric rods can achieve wide bandwidth and allow for design flexibility to produce a desired radiation pattern. With readily available dielectric materials, they can be easily fabricated at a very affordable cost. Tapers of the circular cross section are used to improve bandwidth, as well as control the side lobe level, which is illustrated in details in, e.g. [4] [5] [6]. Nevertheless, at higher frequencies, these rod antennas are hampered by the inevitable appearance of higher-order modes. Higher-order modes kick-in when the rod diameter exceeds the guided wavelength, degrading the pattern and polarization [7]. To overcome this limitation, electromagnetic absorbers and enclosures were used, as shown in [8] in conjunction to a broadband feed, resulting in a 3:1 (2~6 GHz) bandwidth dielectric rod antenna. Moreover, in reference [4], a wider bandwidth design using multiple sections in the rod was reported. Each section in this design was fine-tuned for best wave transmission and radiation throughout the dielectric rod antenna. Furthermore, the feed was exponentially-tapered using a launcher, surrounded by absorbers to reduce the side lobes. As a result, stable patterns and a low reflection coefficient over 4:1 bandwidth (4-18 GHz) was presented [3]. Nevertheless, this design still suffers from several issues, such as low radiation efficiency and an electrically large structure which is almost 3.7 wavelengths at the middle frequency of the band. Moreover, its fabrication is complex, and the antenna achieved a relatively low gain (5dB in average). Nonetheless, the rod antenna in [3] provides the maximum reported bandwidth using a single dielectric layer.

Suppressing the higher-order modes at higher frequencies has been a key focus to improve ultra-wideband performance of circular cross section dielectric rod antennas. Since higher-order modes appear at electrically large cross-sections, multi-layered dielectric rod antennas have been proposed in [9] [10]. A dielectric core with higher permittivity is added to guide electromagnetic energy around the core at higher frequencies. Consequently, the design in [9] was able to achieve more than 4:1 bandwidth by utilizing dielectric two-layers. Moreover, the use of multiple dielectric layers was theoretically examined previously. For example, using three layers, an impressive 9:1 (2-18 GHz) bandwidth was achieved [10], however, a full realization of the 3-layer antenna in [10] has not been reported. The main challenge of the three-layer rod design is its fabrication using traditional dielectric rod fabrication methods due to incompatible mechanical properties among materials with three different dielectric constants.

In this work, a single-layer dielectric rod antenna using a novel V-shaped transverse electromagnetic (TEM) waveguide feeding structure is presented, resulting in 5:1 bandwidth and a much simpler design compared to two-layer dielectric rod antennas. The new feed structure supports a TEM mode over a very large bandwidth that couples effectively into the hybrid dielectric waveguide mode and minimizes the pattern degradation at higher frequencies. In addition, the design maintains high radiation efficiency over the entire 6-30GHz band. The presented dielectric rod antenna consists of three main parts: a launcher, the rod body, and the radiation taper. The design guidelines for each section are described in detail below.

II. Design of The UWB Dielectric Rod Antenna

As noted above, our tapered circular cross-section dielectric rod antenna design consists of three regions that can

This article has been accepted for publication in a future issue of this journal, but has not been fully edited. Content may change prior to final publication. Citation information: DOI 10.1109/TAP.2017.2677379, IEEE Transactions on Antennas and Propagation

be optimized for best performance, as in [4]. As shown in Fig. 1(a), the three sections are referred to as the launcher, the rod body, and the radiation taper. The "launcher" enables the excitation of the dielectric rod antenna via a standard coaxial cable connection and is necessary to couple the incident coaxial transverse electromagnetic (TEM) mode into the hybrid (HE11) mode to ensure low side-lobes and wide bandwidth [11]. Among the different alternatives, the dielectric core twin-wire TEM waveguide presented in [4] achieves an ultra-wide impedance bandwidth and is relatively simple to fabricate. The TEM horn proposed in [3] also exemplifies an effective design which supports dual-polarization. This feed consists of 4 conducting strips, arranged perpendicular to each other, with reciprocating pairs responsible for generating the orthogonal linear polarizations.

Similar designs were also used as the initial stage of circular TEM waveguide feeds for single polarization as shown in Fig. 2 (a). The flare angle "*b*" of the metallic strip is utilized to control the input impedance of the waveguide. Figure 2 (b) presents the input impedance of the circular TEM waveguide at three different widths of the metallic strip, namely, 30°, 60° and 130°. We note that narrower metallic strip leads to a more stable impedance behavior over frequency. As the strip width decreases, better match is achieved, especially, at the high end leading to a higher impedance bandwidth as shown in Fig. 2 (c). However, at high end of the operation band, pattern degradation kicks-in and this design is limited to approximately 4:1 bandwidth. Figure 3(a) illustrates the key shortcoming of the twin-wire design, where, the *E*-plane side-lobes are more pronounced. This behavior is due to the concentration of the propagating energy along the metallic strips. The energy can be better distributed by using wider metallic strips, however, this comes at the expense of narrower operational bandwidth as stated earlier.

Through the examination of the electromagnetic field at the surface of the flared feed arms, we note that the energy density is lower in the middle section of the strip as shown in Fig. 2 (a). As such, one could cut out the mid-section of the strip, forming a V-shaped strip arm, as illustrated in Fig. 3(b). This V-shaped waveguide achieves a more even distribution of the field around the rod.

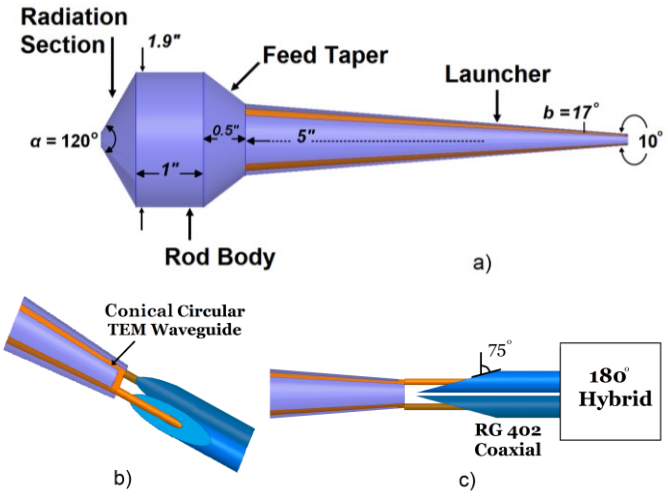

Figure 1: The proposed 5:1 dielectric rod antenna geometry: (a) Side view of the circular rod, illustrating the different sections, (b) The V-shaped twin-wire tapered TEM waveguide used as the launcher, and (c) Differential feeding cables illustrating the Tchebychefff tapered balun transformer.

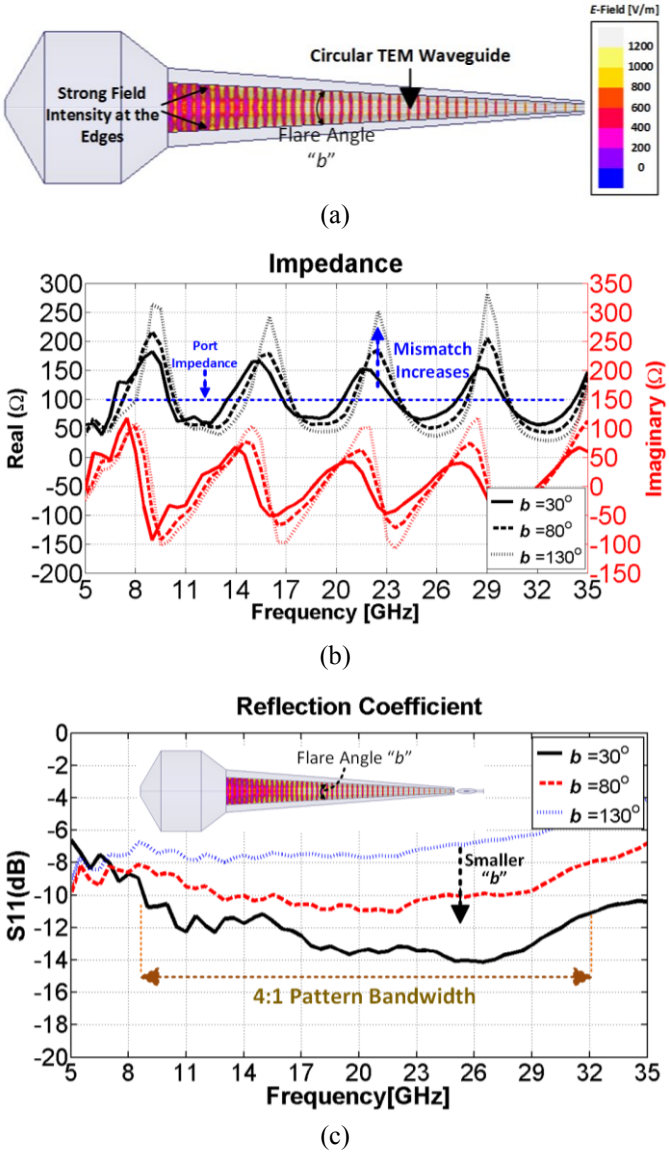

Figure 2: (a) Circular TEM waveguide showing the tangential electric field distribution. (b) Input impedance of the circular TEM waveguide for different flare angles "*b*" of the metallic strips. (c) Reflection coefficient of the circular TEM waveguide for different flare angles "*b*" of the metallic strips.

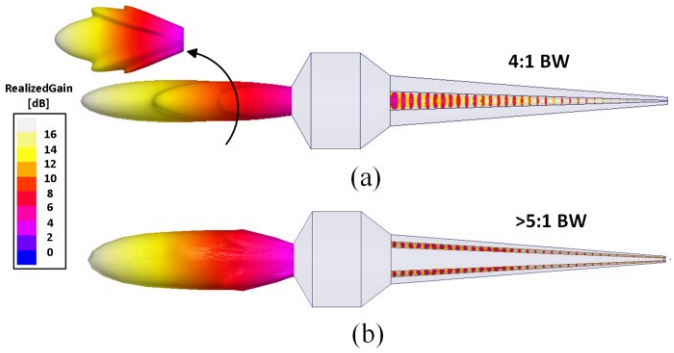

Figure 3: 3D pattern and tangential electric field distribution at 30GHz for: (a) The conventional circular TEM waveguide, and (b) The proposed V-shaped TEM waveguide.

This article has been accepted for publication in a future issue of this journal, but has not been fully edited. Content may change prior to final publication. Citation information: DOI 10.1109/TAP.2017.2677379, IEEE Transactions on Antennas and Propagation

The V-shaped TEM waveguide also brings about several advantages: It reduces the cross-polarization and improves the side lobe levels, and furthermore, it can be readily implemented to support two orthogonal-polarizations, as shown in Fig. 4.

In our final design, the flair angle of the dielectric cone section and the flare angle of the metallic strips are optimized to be 10 degrees and 18 degrees, respectively, resulting in an input impedance of 100 Ω. Detailed analysis of impedance calculations can be found in [12]. Although the presented TEM waveguide looks similar to the one presented in [3], the particular operation and its performance are quite different. In the proposed design, the four arms are grouped into two pairs of adjacent strips and excited concurrently giving this design a symmetrical pattern, matched impedance, and lower cross-polarization. Using two single-pole double-throw RF switch, the grouping can be changed from vertical to horizontal to support the two orthogonal polarizations, albeit not simultaneously (as illustrated in Fig. 4). In contrast, the design shown in [3] consists of four arms that are separated from each other where the pairs are excited simultaneously giving the desired polarization.

To ensure smooth transition between launcher and rod body without exciting high order modes, optimum length of the launcher has to be determined. It is found that a launcher section of $2.5\lambda_0$ is an acceptable choice for best impedance match, where λ_0 is the free space wavelength at the lowest frequency. We note that extending the launcher beyond the feed taper increases the side lobe levels, specifically at high frequencies, thus, it is recommended to stop the launcher right before the feed taper of the dielectric rod antenna.

As seen in Fig. 1, the rod section is purposely large so that evanescent fields from launcher junction attenuate before they reach to the radiating tip. The rod diameter is designed more critically because it controls the field behavior within and outside the rod as shown in Fig. 5. Simply increasing the diameter beyond the largest operation wavelength guides the energy inside the rod, as shown in Fig. 5 (a), therefore, no leaky-wave radiates through the rod body. However, increasing the rod diameter beyond the operation wavelength creates undesired higher-order modes. These modes degrade the pattern and limit the bandwidth [8]. On the other hand, reducing the diameter of the rod beyond the wavelength at a mid-band frequency allows part of the propagating energy inside the rod to leak out at the rod section and radiate into air before it reaches the radiation section as shown in Fig. 5 (c). As such, the remaining part of the energy continues to travel within the rod until it reaches the radiation section, where it radiates through the taper part. Thus, the rod geometry needs to be carefully designed, such that the two parts of the energy radiating from different sections add constructively. Since this condition is difficult to meet at wide range of frequencies, these antennas is usually narrow band. Figure 5 (c) shows one of the scenarios where the leaky-wave radiation at the rod interferes destructively with the field escaping via the radiation sections, leading to field cancelation at end-fire direction. In addition, reducing the diameter beyond the largest wavelength creates a negatively flared rod taper that increases the side lobe level if not carefully designed. Figure 5 (b) shows an intermediate case, where the rod diameter is close to a wavelength. At this point, the leaky-waves attenuate at close distance from the rod, however, increased side lobe level is observed. As a result, the optimum diameter of the rod is slightly higher than free space wavelength at the lowest frequency. Moreover, the resulted outwardly tapered section adds another advantage to the design. It removes the potential of a null in the broadside direction that may typically appear at different frequencies.

The radiation section is the most challenging part of the dielectric rod antenna. The optimum design is achieved through the aid of simulation tools, which are used to minimize the reflected energy, minimize the leaky-wave

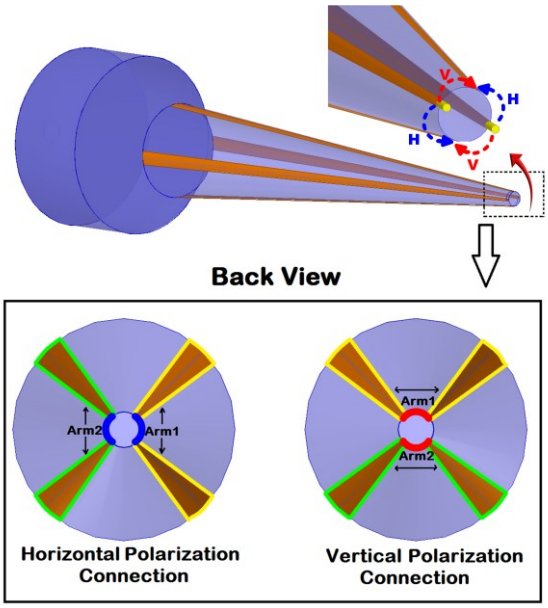

Figure 4: Proposed V-shaped tapered twin-wire TEM waveguide feed structure and pair-wise excitation of the two orthogonal modes to achieve ultra- wideband operation.

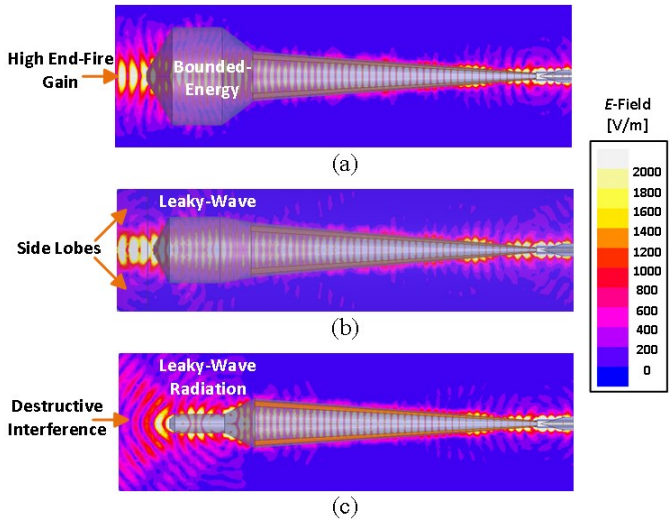

Figure 5: Tangential electric field distribution of the propagating wave outside the rod body at three different diameters of the rod body: (a) Rod diameter is larger than the wavelength, (b) Rod diameter is approximately equal to the wavelength, and (c) Rod diameter is smaller than wavelength.

This article has been accepted for publication in a future issue of this journal, but has not been fully edited. Content may change prior to final publication. Citation information: DOI 10.1109/TAP.2017.2677379, IEEE Transactions on Antennas and Propagation

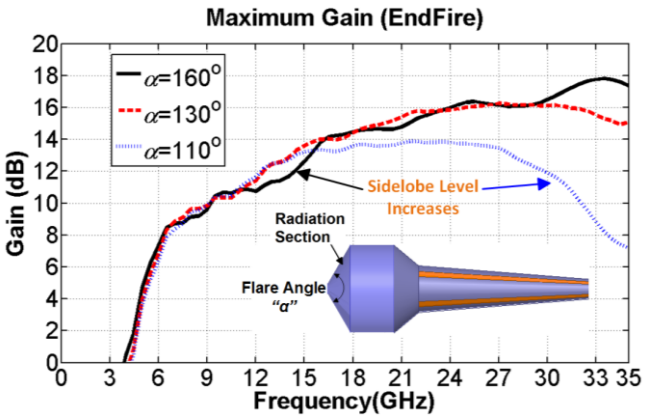

(a)

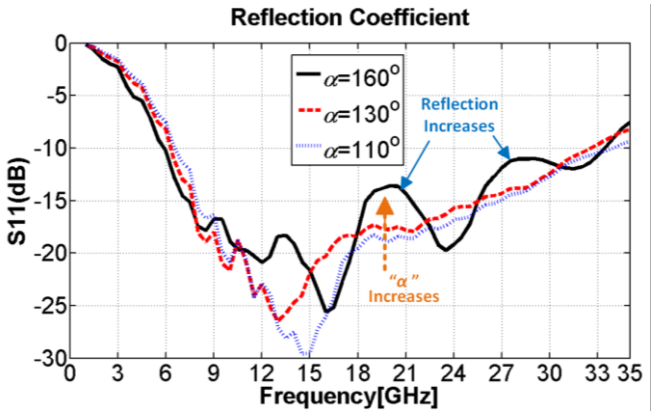

(b)

Figure 6: DRA performance at different flare angles "α" of the radiating section. (a) End fire gain, and (b) Reflection coefficient.

radiation, and minimize diffraction at high frequencies. Figure 6 shows the antenna performance for different flare angles "α" of the radiation section. For a small flare angles, i.e. a smooth taper, the end-fire gain decreases at high frequencies due to an increase in the side lobe level, whereas, at larger flare angles (i.e. sharper taper), sidelobes appear at lower frequency as shown in Fig. 6 (a). Concurrently, the reflected energy increases, leading to reflections in S_{11} as shown in Fig. 6 (b). Through optimization, the cone angle was determined to be 120° and the length is approximately one effective wavelength (guided wavelength in dielectric) at the highest frequency.

The antenna prototype was differentially fed using two 5" long RG402 coaxial cables. Cable loss ranges between 0.3dB at 6GHz- 0.8dB at 35GHz, per manufacturer specifications [13]. To achieve impedance match from coaxial line to balanced line, a Tchebychefff tapered balun transformer is implemented as shown in [14]. The angle cut of the outer conductor is 75° as shown in Fig. 1. The antenna is tested for a single polarization; however, as mentioned before, it has the capability of supporting orthogonal-polarization due to symmetry of the overall topology. Furthermore, the performance of the antenna, including realized gain, radiation pattern and S_{11}, in the orthogonal polarization is going to be similar. This is simply proof by circularly rotating of the antenna by 90° around the rod axis.

(a)

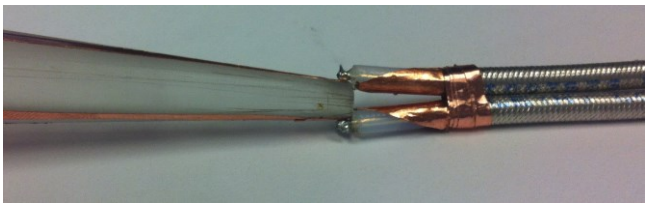

(b)

Figure 7: Fabricated prototype of the 6-30GHz dielectric rod antenna: a) Machined Rexolit_1422 rod body and the V-shaped dual polarization feed strips, b) Tchebychefff tapered balun for coaxial cable interface.

III. Measured Antenna Performance

After optimizing the three aforementioned rod sections for 6-35GHz operation via full wave simulations using Ansoft HFSS V.15 software, the resulting topology was fabricated using Rexolit_1422 material (tan δ = 0.002, ε_r= 2.53), as shown in the Fig. 7(a).

The coaxial balun taper was realized using conducting tape. Similarly, the strip feed taper was implemented using conducting tape which are cut according to the simulation with slight variations in angle and smoothness as shown in Fig. 7 (b). The antenna was fed differentially through a 6-40GHz 180° hybrid with 4.6±1.6 dB coupling. The active, balanced-feed reflection coefficient was measured at the driving point of the antenna, i.e. "Point 2" as shown in Fig. 9 (a) using a 2-port vector network analyzer, and compared with the computed data at the same point. Figure 8 shows the agreement between the simulated and measured active reflection coefficient over the entire design bandwidth. As seen, the measured active reflection coefficient remains below -10dB over the entire band from 6-30GHz. The disagreements at lower frequencies

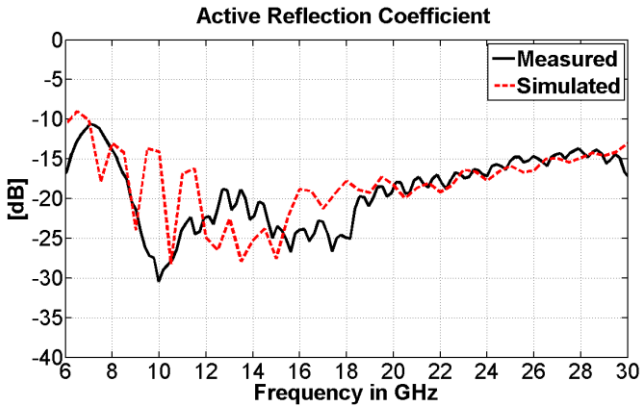

Figure 8: Computed and measured active reflection coefficient of the fabricated dielectric rod antenna at the differential cable feed point 2 as shown in Fig. 9(a).

can be attributed to the fabrication accuracy of the tapered sections of the coaxial feeds.

E- and *H*-plane radiation patterns at different frequencies in the band of interest were also characterized in the anechoic chamber at The Ohio State University. A comparison between the measured and the simulated patterns is shown in Fig. 9 (b). The results demonstrate that the patterns in *E*- and *H*-plane are similar, and the patterns are symmetric. In addition, the measured results agree very well with the simulated design.

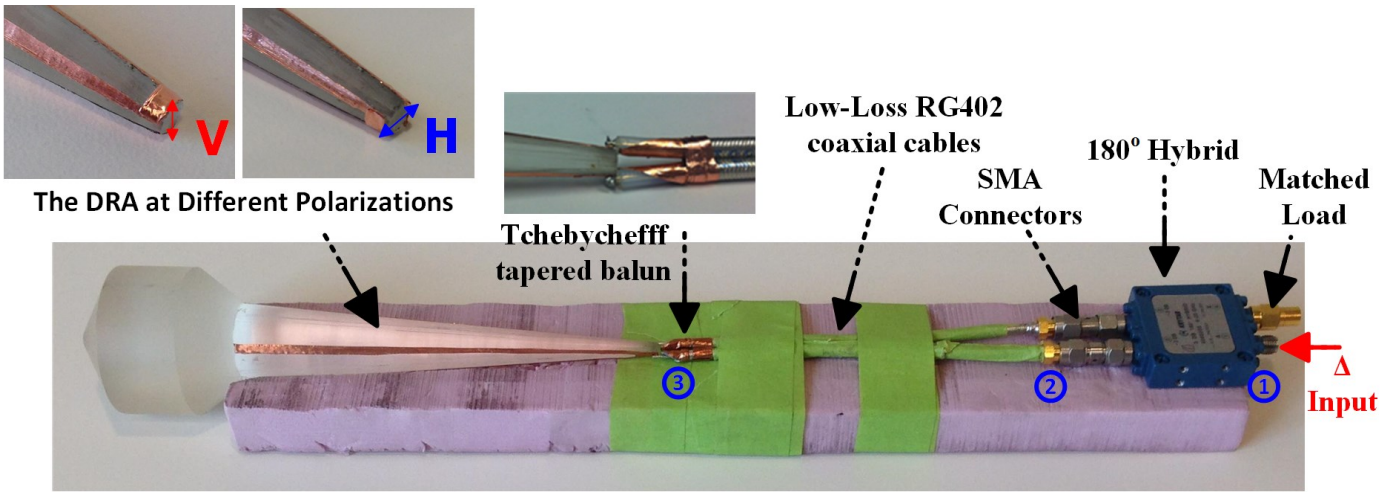

(a)

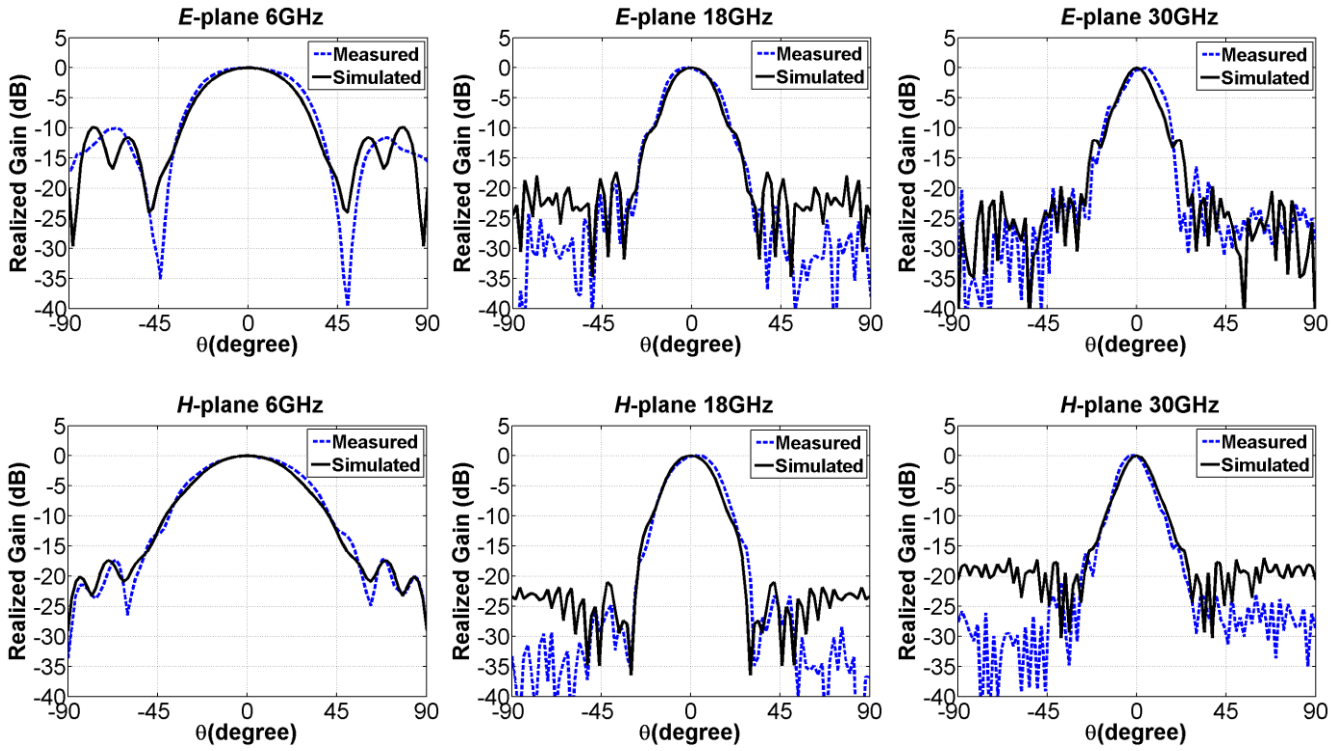

(b)

Figure 9: (a) Measurement setup showing the antenna with the feeding network. (b) Computed and measured radiation patterns of the dielectric rod antenna at representative frequencies for *E*- and *H*-planes.

This article has been accepted for publication in a future issue of this journal, but has not been fully edited. Content may change prior to final publication. Citation information: DOI 10.1109/TAP.2017.2677379, IEEE Transactions on Antennas and Propagation

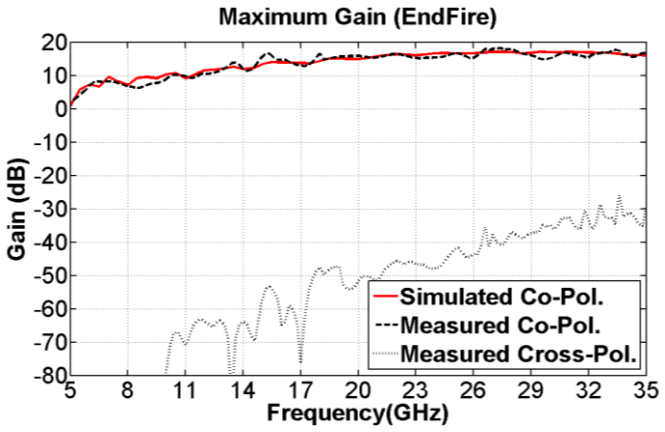

Figure 10: Computed and measured co-polarized and cross-polarized gain of the proposed dielectric rod antenna.

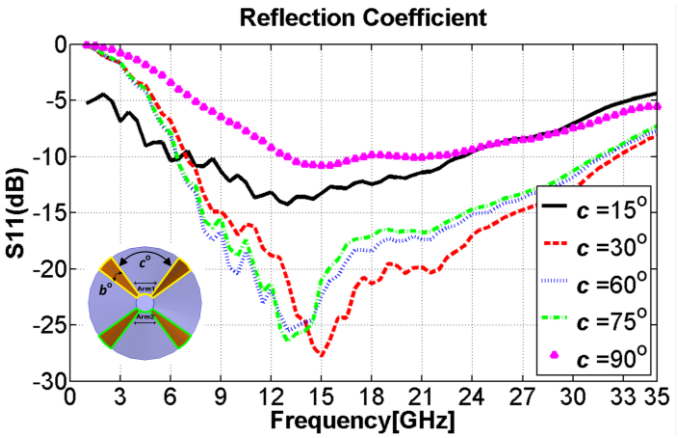

Figure 11: Reflection coefficient of the proposed rod antenna at different separation angles "*c*" between the metal strips, while "*b*" is fixed at 15°.

The end-fire gain is plotted with respect to frequency in Fig. 10, correlating very well with the simulations. The highest achieved gain is around 17dB at the highest frequency, while the minimum gain is approximately 5dB at the lowest frequency of the band.

IV. Dual-Polarized UWB Feed Structure

The novel V-shaped feed waveguide presented above supports over 5:1 bandwidth for two orthogonal polarizations. The design allows switching between the two polarization states, which is particularly useful for near-field probe measurements. However, in many applications, simultaneous dual-polarization operation is desired. This can easily be incorporated into the design process of the V-shaped feed structure detailed above.

A simple modification to the proposed feed is to insert additional V-shaped TEM waveguides that support two orthogonal polarizations. This requires moving the adjacent strips closer to each other, thus narrowing down the separation angle "*c*" in Fig. 11, which leads to increased coupling between the neighboring strips. Therefore, to determine the widest angle "*c*" that can be reached without altering the performance, a parametric study was considered, as shown in Fig. 11. As seen, the optimum value of the "*c*" is approximately 60°, where the strips are furthest from each other from both sides. With this flare angle, the impedance bandwidth is widest and the radiation pattern is symmetric over the band.

As "*c*" deviates from 60°, the antenna performance degrades. At two extremes cases, where "*c*" equals 15° or 90°, the input impedance changes significantly due to the coupling effect, that leads to extremely narrowed bandwidth. However, the angle "*c*" can be reduced to 30° without altering the input impedance significantly, and the impedance bandwidth remains almost the same, as shown in Fig. 11.

Based on this observation, a new launcher with simultaneous dual-polarization capability is implemented using two orthogonal V-shaped TEM waveguides as shown in Fig. 12. The angle "*c*" between the adjacent strips of each waveguide arm is 30°, leaving a flare angle of the metal strip around 15°. Reducing the flare angle of the metallic strip would give wider separation angle "*c*" between the strips, However, it adds negligible improvements on the performance, whereas, it increases the complexity of the fabrication.

A full wave simulation is performed for the antenna in Fig. 12 using the full wave simulator Ansoft HFSS v.15. Both polarizations are excited at the same time using four coaxial cables and corporate feeding network is assumed. Here, corporate network, for simplicity, assumes 1:2 divider/combiner, that is lossless, perfectly matched at all ports, with perfect phase balance and infinite isolation between the output ports. Figure 13 (a) presents the reflection coefficient at the input of the corporate network. As shown, the impedance bandwidth increases when the dual-polarizations are excited simultaneously. The realized end-fire gain is also presented in Fig. 13 (b). The realized gain value has dropped by half, as the power now is divided between the two polarizations. Whereas, the simulated cross-polarization level remains extremely low. This is one of the advantages of the crossed strips in the V-shaped TEM waveguide. Finally, Fig. 13 (c) and (d) present the patterns at the lowest and the highest frequencies of the band, respectively. As noted, the pattern in *E*-plane is slightly wider than in *H*-plane due to the new strip arrangements, namely, the narrowed arm width in the *E*-plane.

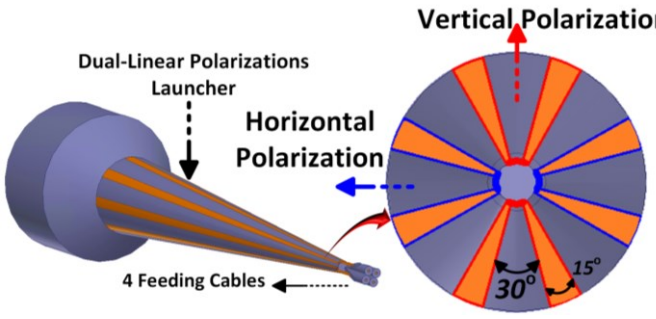

Figure 12: The new launcher design with two orthogonal V-shaped TEM waveguides for dual-polarization performance.

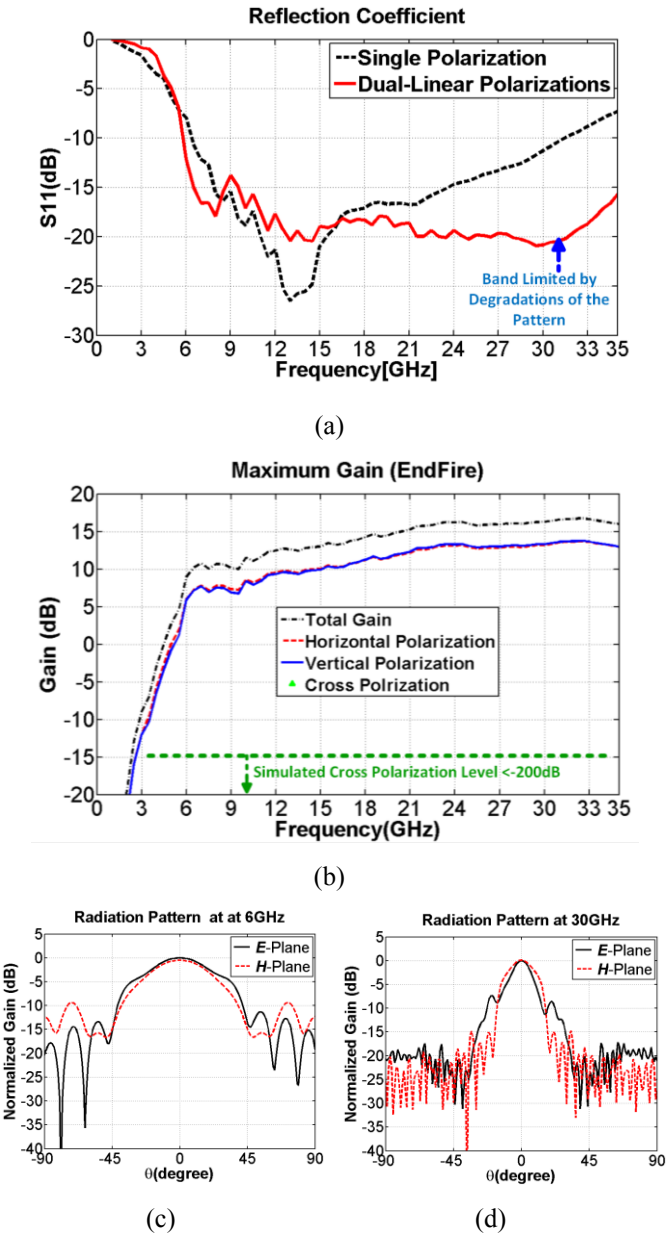

Figure 13: Simulated performance of the dual-linear polarization antenna: (a) Reflection coefficient, (b) Realized gain (end-fire), and radiation patterns at 6 and 30GHz in (c) and (d) respectively.

V. Conclusion

A 5:1 bandwidth, dielectric rod antenna is designed and fabricated for wide bandwidth, high gain, lowest side lobes, symmetric pattern, and dual polarization. The measurements verify excellent performance over the entire band, with a maximum gain of 17dB, -20dB side lobes, and <-10dB reflection coefficient over 6-30GHz. The pattern degradation problems such as symmetricity and nulling, which typically limit antenna operation are tackled by the new V-shaped waveguide feed section, resulting in a dual-polarization, ultra-wide bandwidth, high gain, symmetrical pattern, high radiation efficiency antenna that is simple to build and low cost. It can be used effectively as a near-field probe or a reflector feed.

References

[1] D. G. Kiely, Dielectric Aerials, London: Methuen, 1953.

[2] J.-Y. Chung and C.-C. Chen, "Ultra-wide bandwidth two-layer dielectric rod antenna," in *Antennas and Propagation Society International Symposium*, Honolulu, HI, 2007.

[3] J.-Y. Chung, "Ultra-wideband dielectric-loaded horn antenna with dual-linear polarization capability," *Progress In Electromagnetics Research,* vol. 102, pp. 397-411, 2010.

[4] F. Zucker, "Surface- and Leaky-Wave Antennas," in *Antenna Engineering Handbook*, New York, McGraw-Hill Book Company, 1961, p. Ch.16.

[5] L. B. Felson, "Field solution for a class of corrugated wedge and cone surface," *Polytechnic Inst. Brooklyn, NY, Microwave Res. Inst., Memo 32,* July 1957..

[6] V. I. Talanov, "On Surface Electromagnetic Waves in Systems with Nonuniform Impedance.," *Izvestiia VUZ WVO, Radiofizika.,* vol. 2, no. 1, pp. 132-133, 1959 .

[7] C.-C. Chen, "UWB dielectric rod antenna designs," in *7th European Conference on Antennas and Propagation (EuCAP)*, Gothenburg, 2013.

[8] C.-C. Chen, K. R. Rao and R. Lee, "A new ultrawide-bandwidth dielectric-rod antenna for ground-penetrating radar applications," *IEEE Transactions on Antennas and Propagation,* vol. 51, no. 3, pp. 371-377, 2003.

[9] J. Y. Chung and C.-C. Chen, "Two-Layer Dielectric Rod Antenna," *IEEE Transactions on Antennas and Propagation,* vol. 56, no. 6, pp. 1541-1547, 2008.

[10] C.-W. Liu and C.-C. Chen, "A UWB Three-Layer Dielectric Rod Antenna With Constant Gain, Pattern and Phase Center," *IEEE Transactions on Antennas and Propagation,* vol. 60, no. 10, pp. 4500-4508, 2012.

[11] J.-H. Qiu and N.-N. Wang, "Optimized dielectric rod antenna for millimeter wave FPA imaging system," in *IEEE International Workshop on Imaging Systems and Techniques (IST '09)*, Shenzhen, 2009.

[12] N. V. Venkatarayalu, C.-C. Chen, F. L. Teixeira and R. Lee, "Numerical modeling of ultrawide-band dielectric horn antennas using FDTD," *IEEE Transactions on Antennas and Propagation,* vol. 52, no. 5, pp. 1318-1323, 2004.

[13] "RG402 Cable Specifications M17/130-RG402," EMC Technology & Florida RF Labs, [Online]. Available: http://www.emc-rflabs.com/.

[14] J. W. Duncan and V. P. Minerva, "100:1 Bandwidth Balun Transformer," *Proceeding of the IRE,* vol. 48, no. 2, pp. 156-164, 1960.

Anas J. Abumunshar (GS'16) was born in Hebron, Palestine in 1986. He received his B.Eng. degree in Telecommunications from Mu'tah University, Jordan, in 2008, and his M.Sc. degree in electrical engineering from University of Bridgeport, CT, USA, in 2012. Anas is currently working towards his Ph.D. degree in electrical engineering at The Ohio State University.

During his master, he was a student researcher at the signal processing research lab at University of Bridgeport, CT, USA. Since 2013, he has been a Graduate Student Researcher with the ElectroScience Laboratory at The Ohio State University. His research interest includes phase-array systems, ultra-wideband arrays, and microwave/millimeter-wave circuit designs. He is also interested in, speech signal processing for automatic accent detection and enhanced speech recognition, and the inter-relation between sound and magnetic waves.

Kubilay Sertel received his PhD in 2003 from the Electrical Engineering and Computer Science Department at the University of Michigan-Ann Arbor. He is currently an Assistant Professor at the Electrical and Computer Engineering Department at the Ohio State University. He was a Research Scientist at the ElectroScience Laboratory and an Adjunct Professor at the Electrical and Computer Engineering Department at the Ohio State University during 2003-2012. His current research focuses on the analysis and design of THz and mmW sensors, antenna arrays and on-wafer non-contact metrology systems for device and IC testing as well as spectroscopy techniques for biomedical and non-destructive imaging. His research interests also include ultra wideband low-profile phased arrays for cognitive sensing and opportunistic wireless networks, reconfigurable antennas and arrays, applied electromagnetic theory and computational electromagnetics, particularly, curvilinear fast multipole modeling of hybrid integral equation/finite element systems and efficient solution of large-scale, real-life problems on massively parallel supercomputing platforms.

Prof. Sertel is a Senior Member of IEEE, member of IEEE Antennas and Propagation and Microwave Theory and Techniques Societies and an elected member of URSI Commission B. He is a Fellow of Applied Computational Electromagnetics Society. He is also the Editor-in-Chief for Electronic Publications for the IEEE Antennas and Propagation Society. He co-authored two books: *Frequency Domain Hybrid Finite Element Methods in Electromagnetics* (Morgan & Claypool, 2006), and *Integral Equation Methods for Electromagnetics* (SciTech Publishing, 2012), 6 book chapters, 3 patents, and published 79 journal papers and over 260 conference articles.